Full paper

Quantifying the power output and structural figure-of-merits of triboelectric nanogenerators in a charging system starting from the Maxwell's displacement current

Jiajia Shao[a,b], Morten Willatzen[a,c], Tao Jiang[a,b], Wei Tang[a,b], Xiangyu Chen[a,b], Jie Wang[a,b], Zhong Lin Wang[a,b,d,*]

[a] CAS Center for Excellence in Nanoscience, Beijing Key Laboratory of Micro-nano Energy and Sensor, Beijing Institute of Nanoenergy and Nanosystems, Chinese Academy of Sciences, Beijing 100083, China
[b] College of Nanoscience and Technology, University of Chinese Academy of Sciences, Beijing 100049, China
[c] Department of Photonics Engineering, Technical University of Denmark, Kongens Lyngby, DK-2800, Denmark
[d] School of Materials Science and Engineering, Georgia Institute of Technology, Atlanta, GA 30332-0245, United States

ARTICLE INFO

ABSTRACT

Conversion of mechanical energy into electricity using triboelectric nanogenerators (TENGs) is a rapidly expanding research area. Although the theoretical origin of TENGs has been proven using the Maxwell's displacement current (I_D), a profound quantitative understanding of its generation is not available. Moreover, a comprehensive analysis of the fundamental charging behavior of TENGs and building a standard to evaluate each TENG's unique charging characteristic are critical to ensure efficient use of them in practice. We present a thorough analysis of TENG's charging behavior through which a more complete evaluation of TENG charging is proposed by introducing the structural figure of merit (FOMC) in a charging system (powering capacitors). The analysis is based on Maxwell's displacement current and results are verified experimentally. To achieve this, according to the distance-dependent electric field model, we provide a systematic discussion on the generation of I_D in TENGs, along with the derived analytical formula and numerical calculations. This work suggests a new way to deeply understand the nature of the I_D generated within the TENGs; and the modified FOM_S can be used to predict the charging characteristics of TENGs in an energy storage system, allowing us to utilize the TENGs more efficiently towards different applications.

1. Introduction

To eliminate the inconsistency between Ampere's law and the principle of conservation of charges, the displacement current (I_D) was first proposed by James Clerk Maxwell in 1861, by adding a changing electric field as the source of the magnetic field [1]. The displacement current is not the current produced by flow of free charges, but originates from a time-varying electric field and the associated media polarization [1,2]. Triboelectric nanogenerators (TENGs) are typically composed of two electrodes and at least one pair of triboelectric layers [3–7]. The I_D is generated due to the horizontal/vertical movement of these layers with opposite triboelectric charges [8]. These triboelectric charges caused by the electron, ion, or material transfer, lead to a time-varying electric field between the two electrodes when the TENG is driven by mechanical action [9–13]. The time-varying electric field propagates through the dielectric, until it is shielded by the free (induced)

charges at the dielectric-electrode interface. During the process, the electric flux changes over time leading to the generation of I_D. In other words, the fundamental theoretical origin of TENGs is the Maxwell's displacement current, and the TENG represents the application of Maxwell's displacement current in energy and sensors [8,14–18]. Hence, developing a comprehensive discussion of the generation of I_D, along with its affecting parameters based on the time-varying electric field, is a key priority in-depth understanding the nature of TENG.

Immediate and effective conversion of mechanical energy into electricity is an essential characteristic of TENGs. However, owing to the irregular and uncontrollable performances of the driven source, such as wind, waves, and other ambient sources, the generated electrical output is unstable and usually shows a high voltage but limited current and thus can't be utilized directly to power electronic devices and sensor networks [19–23]. Hence, an energy storage unit is required to store the generated electricity,
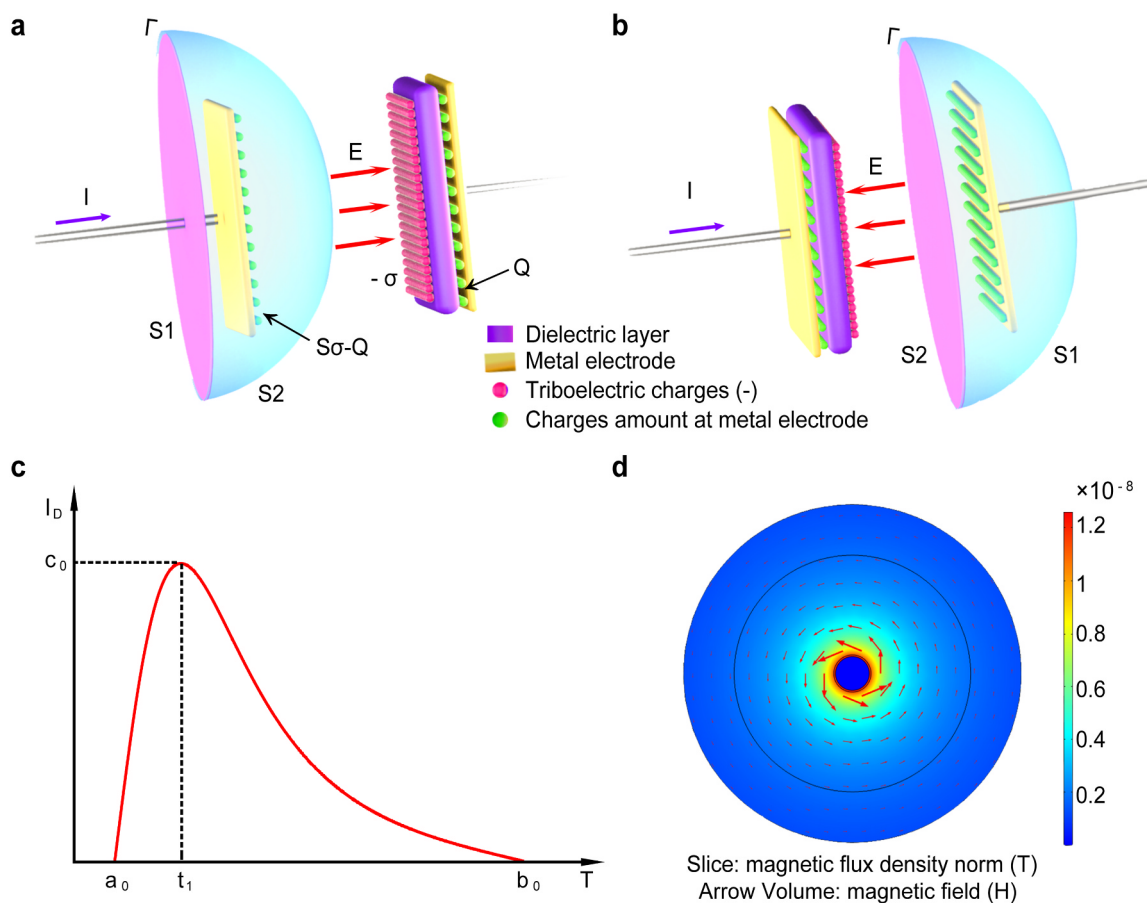

Fig. 1. Illustrations about the Maxwell's displacement current (I_D) and the magnetic field at a distance r from the conducting wire for a vertical contact-separation (CS) triboelectric nanogenerator (TENG). (a, b) Defined surfaces S1 and S2 near the metal electrode of the TENG are bounded using a same path Γ. The conduction current I passes through S1 but not through S2, only the displacement current I_D passes through S2. The two currents are equal and continuous. Note that the transferred charge between the two electrodes is Q. (c) The typical I_D between the metal electrodes of the CS mode TENG varies with time and has a maximum value, when the TENG is subject to sinusoidal motion. (d) The distribution of the magnetic field at a distance r from the conducting wire: the slice shows the magnetic flux density norm; the arrows indicate the magnetic field (H) strength and direction.

with the aim of providing a stabilized and manageable output through a capacitor or battery. While most of the previous reports have focused on the theoretical prediction of the energy generation process, the energy storage step, which is a central point, has drawn less attention [24–29]. From previous limited studies, we can obtain only a few basic charging characteristics of TENGs [30,31]. For instance, an optimum load capacitance exists at which the energy transfer reaches a maximum otherwise a large proportion of potentially usable energy may end up being wasted due to capacitance mismatch between the TENG and the energy storage unit. Many other fundamental behaviors such as the current and power output could not be predicted which impeded efficient use of the TENGs. In addition, many types of TENGs have been designed and fabricated, and each mode has its own structure and related driven configurations [32–36]. To assess and evaluate each TENG's charging characteristic especially at different load capacitances is an important task to address.

In this work, we present a comprehensive analysis of using a TENG to charge a capacitor and provide, for the first time, a predictable way to understand the current and power behavior based on which a standardized evaluation of the charging characteristics of TENGs, *i.e.*, the structural figure of merit in a TENG charging system (FOMC$_S$) is proposed. In accordance with Maxwell's equations, the generation of Maxwell's displacement current and its influencing factors are fully investigated based on the distance-dependent electric field model. After that, the fundamental charging characteristics of TENGs are described with (or without) a full-wave bridge rectification, such as the current and power, along with the consideration of charging cycles, maximum distances and other affecting parameters. Finally, the structural FOMC$_S$

is presented, which is utilized as a standard to evaluate and predict the TENG's charging performances in an energy storage system, and through which a TENG's performance can be fully assessed.

2. Theory

2.1. Energy conversion and capacitive model

Triboelectricity happens between two different materials that are brought into contact and separated. Its mechanism is typically contributed to electron transfer, ion transfer and/or material transfer mainly determined by the respective work functions [9–13]. When having physical contact, materials with a high work function accepts easier electrons from materials with a low work function, so that two different dielectric materials create oppositely charged surfaces, producing a contact potential difference between them [37]. The electron transfer will fade away as the Fermi levels of the two materials approach each other at contact. Before that, a potential difference is beneficial to put the charged surfaces together. Separation of them, combined with the induction due to the movement of these layers, needs work done by a driving force whereby mechanical motion is converted into electricity. However, because of dielectric materials' poor conductivity, tribo-charges are static charges that cannot move freely, and any charge loss will be replenished by the new contacts [28,29,37]. So that, after several driven cycles, triboelectric surface charge density increases and saturates, finally establishing a steady state. Therefore, we assume that the tribo-charges are uniformly

distributed on the contacting surfaces, and these charges remain unchanged even when the oppositely charged surfaces are separated. This is a fundamental theoretical principle behind all TENG models which have already proved to be accurate by comparison with experimental results [9,11,38–40].

The first physical model of a TENG is the capacitive model which is established based on the electric field perpendicular to an infinitely large electrode, because the area size of the electrodes is a few orders of magnitude larger than their separation distance [26]. Then, the resultant electric field between the two charged surfaces becomes σ/ε_0, elsewhere it is zero. This model has a certain success in explaining the unique characteristics of TENGs, through which the standards of TENGs have been built up [41]. Another model is the distance-dependent electric field model [29], through which the total electric field above the midpoint along an axis of a finite charged plane with length and width can be derived [See ESI, Supplementary Note 1]. A variation in the electric field with the distance from a finite charged plane is consistent with the actual conditions of TENGs.

2.2. Generation of displacement current

According to Maxwell's electromagnetic field theory, the time-varying electric field will result in electric flux changes over time leading to the generation of a displacement current [1,2]. This phenomenon can be interpreted mathematically through a CS mode TENG illustrated in Fig. 1a-b. As tribo-charges on the contacting surfaces reach a steady-state, free charges induced on the electrodes will flow through the external circuit, producing an alternating current (AC) conduction current I.

Now considering the two surfaces S_1 and S_2, bounded by the same path Γ (Fig. 1a). Ampère's law states that $\oint \mathbf{B} \cdot d\mathbf{s}$ is $\mu_0 I$ because the conduction current I passes through S_1. If the path is considered as bounding S_2, no conduction current passes through it, but there exists the displacement current. We can make the surface S_2 in Fig. 1a (1b) into a "special Gaussian surface", which is everywhere perpendicular to the total electric field between the charged surfaces and over which the electric field is uniform. The displacement current through a surface S which passes the dielectric in Fig. 1a is:

$$\mathbf{I}_D = \int_S \frac{\partial \mathbf{D}}{\partial t} \cdot d\mathbf{a} = \frac{\partial}{\partial t}\left(\int_S \mathbf{D} \cdot \mathbf{n} da\right) = \frac{\partial}{\partial t}\left(\int_S \varepsilon_0 \varepsilon_r \mathbf{E} \cdot \mathbf{n} da\right) = \frac{\partial Q}{\partial t} \tag{1}$$

where ε_r is the dielectric constant, Q is the transferred charge (free charge). Note that for an isotropic material, the relationship between $\mathbf{D}$ and $\mathbf{E}$ is $\mathbf{D} = \varepsilon_0\varepsilon_r\mathbf{E}$ [1,2] (See ESI, Supplementary Note 2). Further, I_D equals the conduction current in the external circuit of TENGs. Based on the postulation of the displacement current, the contradictory situation that arises from the discontinuity of the current is solved. In other words, when the path Γ is considered as bounding S_2, $\oint \mathbf{B} \cdot d\mathbf{s}$ is not zero, due to the displacement current I_D passing through it. Note in particular, as a TENG is driven by a mechanical force, the changing electric field between the two electrodes is equivalent to the conduction current in the external circuit. A second term $\partial \mathbf{P}/\partial t$ in I_D is related to the polarization of the media plus the electrostatic charges arising from piezoelectric or triboelectric effects, from which the fundamental characteristics of piezoelectric nanogenerator and triboelectric nanogenerator can all be derived [8]. Therefore, an additional term $\mathbf{P}_s$ due to surface charges should be added, that is $\mathbf{D} = \varepsilon_0\varepsilon_r\mathbf{E} + \mathbf{P}_s$. Hence, for the nonlinear materials, we can also find the displacement current

$$\mathbf{I}_D = \frac{\partial}{\partial t}\left(\int_S (\varepsilon_0\varepsilon_r \mathbf{E} + \mathbf{P}_s) \cdot d\mathbf{a}\right) = \frac{\partial Q}{\partial t} \tag{2}$$

The above analysis provides a systematic mathematical demonstration of the generation of I_D in a TENG.

2.3. Power output and energy transmission

Consider a CS mode TENG connected to an external capacitor (C_L). We start with a simple case where the C_L is charged under a unidirectional mechanical motion (Fig. 3a). Because the charging current is unidirectional no rectifier bridge is needed during the charging process. However, in real practical applications, TENGs usually work under periodic mechanical motion, outputting the AC current. This AC current is typically converted to direct current (DC) to power storage unit by a full-wave bridge rectifier (Fig. 3b). In general, when a voltage is applied to a conventional C_L, opposite free charges will be generated and stored in electrical conductors. Nonetheless, there are no electric charges transporting through the internal capacitor due to these electrical conductors being separated by a dielectric. This displacement current is indistinguishable from the conduction current I in the external circuit. Its magnitude is proportional to the rate at which the voltage (V^C) across the capacitor varies in time, or, mathematically, $I = C_L dV^C/dt$. In addition, we have proved that the displacement current I_D in a TENG is equal to the conduction current through the external circuit, i.e.,

$$I_D = I = C_L \frac{dV^C}{dt} \tag{3}$$

As stated before, one operation cycle of a TENG can be divided into two half cycles, the first (1st) half cycle and the second (2nd) half cycle. Based on the node charge conservation, Kirchhoff's law and the above analysis the governing equation for the first half cycle can be derived (ESI, Supplementary Note 2). Then, the capacitor current at the first half cycle ($I_{C\,k,1st}$) becomes:

$$I^C_{k,1st} = C_L \frac{dV^C_{k,1st}}{dt} = \frac{dQ^C_{k,1st}}{dt} \tag{4}$$

where, $V_{C\,k,1st}$ represents the voltage across C_L, $Q_{C\,k,1st}$ is the stored charge on C_L, $Q_{k,1st}$ denotes the transferred charges (free charges) from one electrode to the other; k, 1st means at the first half of the kth cycle (ESI, Supplementary Note 3). It should be noted that the voltage across the terminals of the C_L cannot change instantaneously, because such a change (Eq. (4)) would produce an infinite current. Then, we can derive the power ($P_{C\,k,1st}$) and energy ($E_{C\,k,1st}$) stored in the C_L at the first half cycle,

$$P^C_{k,1st} = I^C_{k,1st} V^C_{k,1st} = C_L V^C_{k,1st} \frac{dV^C_{k,1st}}{dt} \tag{5}$$

$$E^C_{k,1st} = \frac{1}{2}C_L(V^C_{k,1st})^2 = \int_{kT}^{\left(k+\frac{1}{2}\right)T} P^C_{k,1st} dt \tag{6}$$

Similarly, at the second half cycle of the kth cycle, the current ($I_{C\,k,2nd}$), power ($P_{C\,k,2nd}$) and energy ($E_{C\,k,2nd}$) stored in C_L can be described (see the ESI, Supplementary Note 3). In particular, the stored energy can be obtained by:

$$E^C_{k,2nd} = \frac{1}{2}C_L(V^C_{k,2nd})^2 = \int_{kT}^{\left(k+\frac{1}{2}\right)T} P^C_{k,1st} dt + \int_{\left(k+\frac{1}{2}\right)T}^{(k+1)T} P^C_{k,2nd} dt \tag{7}$$

Several key observations can be made from the above equations. First, the capacitor current through C_L is I_D, and its magnitude is equal to the conduction current I in the wire or external circuit. So currents flow in a closed circuit. Second, Eqs. (1) and (2) establish expressions for the currents in a TENG in agreement with Eq. (4) and (S30). Third, Eqs. (3)–(7) are generally applicable to other types of TENGs with suitable modifications to C_L and V_{OC} depending on the respective device architecture.

2.4. Structural figure-of-merits in a TENG charging system

Through Eqs. (6) and (7), we can accurately predict the energy storage behavior in C_L powered by TENGs with different configurations. According to the established standards of TENGs, we notice that the
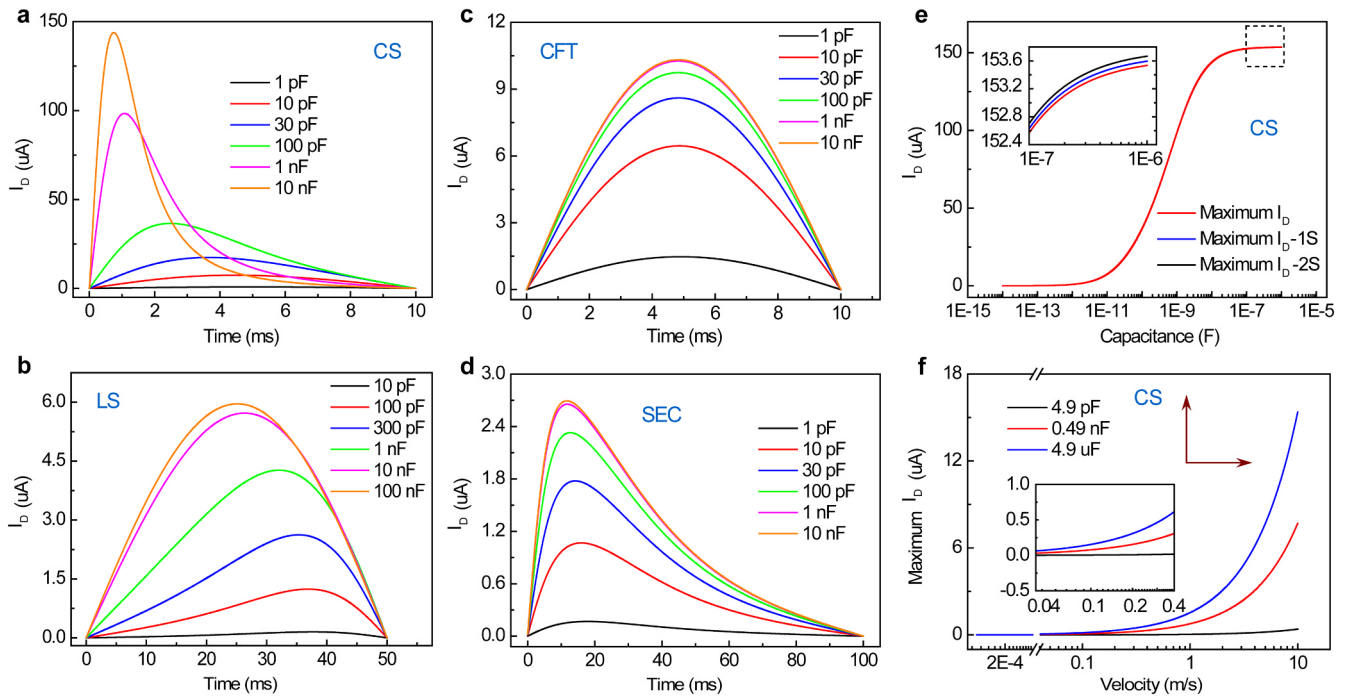
Fig. 2. I_D-time relationships at different load capacitances for (a) CS mode, (c) contact freestanding triboelectric-layer (CFT) structure, (d) single-electrode contact (SEC) structure and (b) lateral sliding (LS) mode TENG calculated by analytical formulas. (e) The influence of the load capacitances on the maximum I_D of the CS mode TENG. The inset shows the change of these maximum I_D when edge effects are considered, whereas the 1S and 2S represent calculations considering 1-side and 2-side effects. (f) Maximum I_D profile with three typical external capacitors (4.9 pF, 0.49 nF and 4.9 µF) at different velocities.

unique output performance of TENG is significantly related to the term of E_m, the largest possible output energy per cycle [41]. However, E_m is quite different from the maximum stored energy $E_{C m}$ in C_L under the same conditions. Mathematically, E_m can be calculated from the maximum short-circuit transferred charge $Q_{sc,max}$, the maximum open-circuit voltage $V_{oc,max}$, and the maximum achievable absolute voltage V_{max} at $Q = Q_{sc,max}$. The $E_{C m}$ is the energy stored in C_L in the final cycle (at saturation voltage V_{sat} of C_L), which is equal to the integral of stored power from 0 to the final cycle time, or the product of C_L and V_{sat}. From previous research, we find that V_{sat} is only a function of TENG parameters, and can be calculated by the equation: $V_{sat} = Q_{SC,max} / (C_{min} + C_{max})$ [31]. Hence, $E_{C m}$ is mainly related to the final charging cycle numbers k and the saturation voltage V_{sat} of the C_L.

On the other hand, the $E_{C m}$, just like the E_m, is also strongly affected by the area of the tribo-charged surfaces (A), maximum relative distance (x_{max}) as well as the surface charge density (σ). Therefore, to quantitatively evaluate each TENGs' unique charging performance, the structural figure of merit in a TENG charging system (FOMC) is proposed, which is affected by the structural parameters, x_{max}, and the final changing cycle numbers k, defined as:

$$FOMC = \frac{2\varepsilon_0}{\sigma^2} \frac{E_m^C}{kAx_{max}} \qquad (8)$$

where, ε_0 is the permittivity of the vacuum, E_m^C represents the maximum stored energy in C_L at the final charging cycle k, which can be calculated by Eq. (7). In other words, the established standards of TENGs could be expanded to be utilized in a charging system, along with appropriate changes. Hitherto, the literature has focused on the available and practical energy stored in C_L based on the practical use of TENGs in a charging system (at powering capacitors), hence disparate conclusions are often made compared with the standard derived FOMs. Here, two points are important to note: first, the structural FOMC is a non-dimensional parameter, which is mainly used in a TENG charging system with the aim of assessing TENG's unique charging characteristics. Further, this structural FOMC highly depends on the TENG structural parameters and final charging cycle, but it is independent of

C_L, which will be demonstrated below. Three, the E_m^C we utilized can be practically achieved in a TENG charging system, thus the corresponding derived FOMCs are also easily attainable and achievable, improving its applicability to predict and assess the charging characteristics of TENGs.

3. Materials and methods

The CS mode TENG was fabricated by attaching a copper (Cu) film as electrode on a fluorinated ethylene propylene (FEP) layer, then the composite layers were attached on an acrylic board, along with the Cu surface facing the board. The Cu layer attached on another acrylic board was utilized as the second triboelectric surface. The TENG layers were contacted and separated through a linear motion control setup. For the LS mode TENG, the fabricated composite layers (Cu/FEP) were utilized as the static part, while the Cu layer attached on another acrylic board was utilized as the motion part. The charge and current outputs were measured using a Keithely 6514 electrometer, whereas the voltage was measured using an oscilloscope. The theoretical calculations of TENG were conducted through the derived equations presented in the article. A typical movement of the TENG layers is achieved by sinusoidal motion profiles defined as $x(t) = 0.5\, x_{max} (1 - \cos(\pi v t / x_{max}))$, where $x(t)$ is the separation of TENG layers at time t, x_{max} is the maximum relative distance, unless otherwise stated.

4. Results and discussion

4.1. Influence of the load capacitance on the displacement current

The real-time I_D for four basic modes of TENGs under unidirectional mechanical motion with different C_L are plotted in Fig. 2. We note that for any external C_L, a current peak exists. Increasing the C_L increases the maximum I_D which is observed for all basic modes of TENGs (Fig. 2a-d). Due to the limited charge transfer rate effected by the capacitive impedance associated with C_L, the output charge does not saturate immediately, leading to the unstopped charge transfer between two
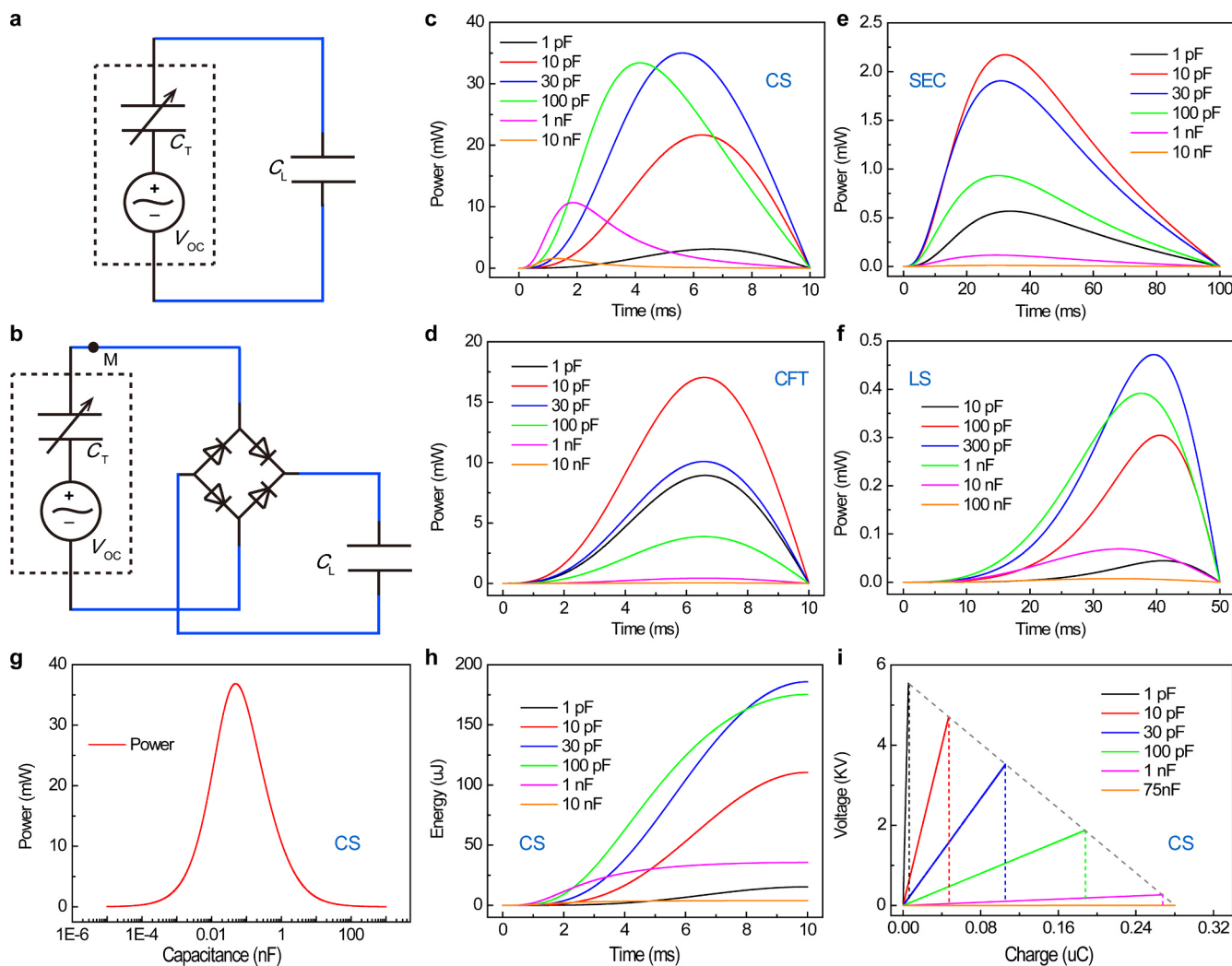
Fig. 3. (a) Equivalent circuit model of a TENG system utilized in the unidirectional charging motion and (b) using a full bridge rectifier to charge a capacitor directly under periodic mechanical motion. Power-time relationships at different load capacitances for (c) CS mode, (d) contact freestanding triboelectric-layer (CFT) structure, (e) single-electrode contact (SEC) structure and (f) lateral sliding (LS) mode TENG calculated by analytical formulas (Eqs (5) and S31). CS mode TENG charging characteristics under unidirectional mechanical motion at the first separation half-cycle: (g) the influence of the load capacitances on the instantaneous power output; (h) stored energy-time relationships at different load capacitances; (f) the encircled areas of V-Q curves with different load capacitances, equivalent to the final stored energy in the first half cycle. Note that all the curves in Figs. 3(c) to 3(i) are numerically calculated under unidirectional charging motion.

electrodes after the triboelectric layers stop movement. Consequently, a peak/maximum I_D is achieved. Furthermore, since the impedance of a capacitor is inversely proportional to C_L, for a particular change in voltage across the capacitor, the smaller the value of the C_L, the bigger the resulting impedance. Therefore, when a very small C_L is loaded, it generates a rather high opposition. This will reduce the electron transfer rate from one electrode to the other, decreasing the change of total electric field between them. As indicated by Eqs. (1) and (2), the reduced change of electric field leads to a lower change of electric flux, resulting in a small I_D. Herein, the rearrange rate of electrons on electrode and the time-varying polarization in dielectric material also slow down. Conversely, if the load C_L increases, the related electric field and electric flux show drastic changes, generating a larger I_D.

As shown in Fig. 2e, it is apparent that increasing C_L results in a significant increase in the maximum I_D until a threshold value but a TENG works close to a quasi-SC condition due to the rather small impedance caused by the larger C_L. Note that edge effects are considered and calculated by analytical formulae (see the ESI, Supplementary Note 5) [25,41]. Except for the C_L, increasing v is also an effective way to improve the maximum I_D (Fig. 2f). This is because the increase of velocity for a given x_{max} corresponds to increasing the frequency of TENGs, *i.e.*, an increasing change in the electric field and electric flux as

well as the maximum I_D. Hence, loading with a larger C_L or increasing v of the triboelectric layers and even both of them can be a suitable strategy to obtain a maximum I_D.

4.2. Power and energy output at unidirectional mechanical motion

Power and energy output of the TENG are important parameters for its use as a power source. The energy stored in different C_L during a TENG half-cycle movement can be accurately calculated by integrating the corresponding output power with respect to time. Fig. 3a is an equivalent circuit model of a whole TENG charging system, and 3b shows that a full bridge rectifier is introduced to charge the C_L directly. For a CS mode TENG, the detailed profiles of the charge, voltage, power, and energy relationships under different C_L are demonstrated in Fig. S3, S4a, S4b, 3c, 3g and 3h, respectively. The corresponding capacitor current calculated under the same conditions can be seen in Fig. 2a. This is because all currents, including the I_D and I, flow in a closed circuit as stated before. We notice that when C_L is small, its impedance is much larger than the impedance of C_T (the time-variant capacitance of the TENG) and the TENG is working under a quasi-OC condition. Hence, the voltage across the C_L is close to V_{OC}. However, due to the slow change rate of dv/dt, the corresponding current is rather
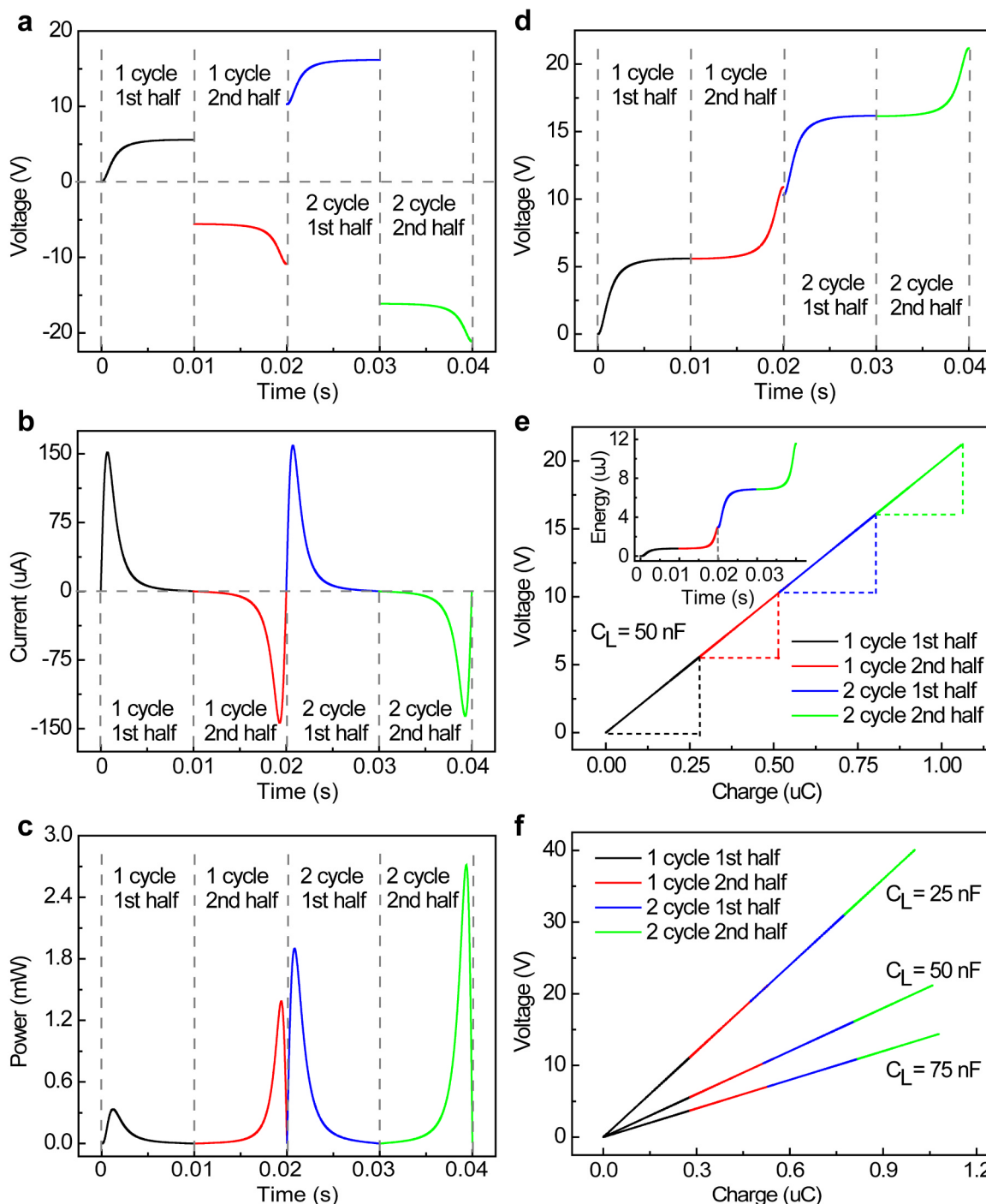
Fig. 4. TENG charging characteristics in the first two cycles. (a) Voltage-time, (b) current-time and (c) power-time relationships with load capacitance C_L = 50 nF. (d) Absolute values of the voltage-time relationships with load capacitance C_L = 50 nF. (e) The *V-Q* curves with load capacitance C_L = 50 nF, the inset is the stored energy-time relationship with load capacitance C_L = 50 nF. (f) The *V-Q* curves with three different load capacitances: C_L = 25 nF, 50 nF and 75 nF.

small. Moreover, a small C_L means that only a limited charges can be stored in it, therefore resulting in a very small stored energy. Conversely, when C_L is rather large, the TENG works under a quasi-short circuit (SC) condition. Although the maximum current approximately approaches the SC current, the voltage applied to the C_L drops to nearly zero, resulting in relatively lower peak power and stored energy. The same situation can be found in other three modes of TENGs, as depicted in Fig. 3d, e and f.

When C_L is neither too large nor too small, the behavior of the TENG is in the transitional region between SC and OC conditions (Fig. S4), within which the maximum power as well as the largest stored energy

can be reached, as shown in Fig. 3g and S4b, respectively. In addition, based on the previous research, we find that the energy output of TENG can be represented by the plot of built-up voltage *V* against the transferred charges *Q* [41]. A similar method was carried out to find the energy stored in C_L through the *V-Q* plots (Fig. 3i). We note that the circled areas of these plots increase firstly and then decrease, demonstrating the largest area at a corresponding C_L, *i.e.*, the optimum C_L of the charging system (here it closes to 30 pF). In order to further prove this result, the *V-Q* plots of the other three modes (CFT, SEC and LS) and the related real-time voltage and charge are also provided, as shown in Fig. S4c-k, which demonstrate a common phenomenon. Therefore, the
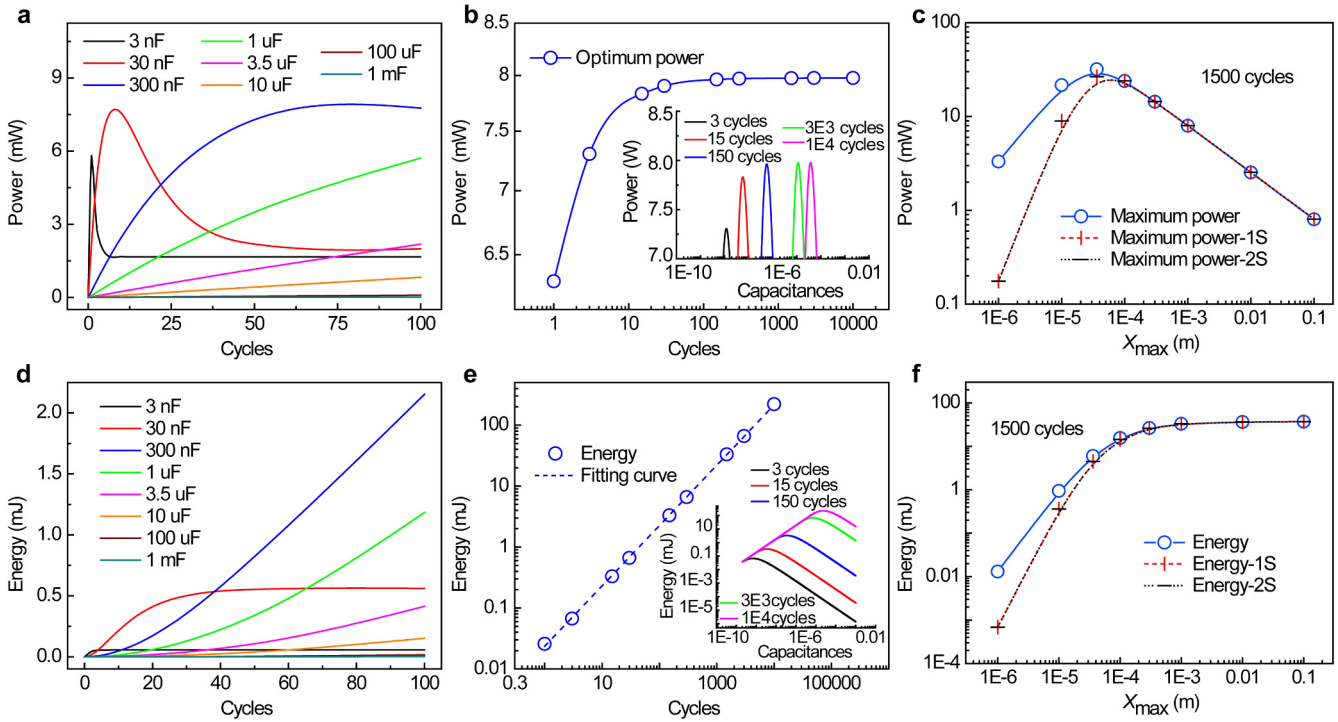
Fig. 5. TENG charging characteristics under periodic mechanical motion. (a) Influence of the C_L on the peak/maximum power at different cycle numbers. (b) Extracted optimum power with different cycle numbers. The inset is the relationship between power and load capacitance at different charging cycles. (c) Extracted optimum power with various x_{max}. (d) Influence of the load capacitance on the stored energy at different cycle numbers. (e) Extracted maximum stored energy with different cycle numbers. The inset is the relationship between stored energy and load capacitance at different charging cycles. (f) Extracted maximum stored energy with various x_{max}. 1S and 2S correspond to calculations considering 1-side and 2-side effects of the CS mode TENG.

V-Q plots presented here could be an effective way to help to understand the energy storage behavior of TENGs.

4.3. Power and energy output under periodic mechanical motion

In practical applications, the TENG is mostly driven under a periodic mechanical motion, leading to the generation of AC voltage/current output. A full bridge-rectifier is utilized not only to transfer these AC signals to DC outputs, but also to prevent charges leaking back from C_L to the TENG, which complicate the electric circuit of the TENG charging system. To systematically analyze the whole process, several problems need to be taken into account. First, the conversion process, involving four diodes in the bridge configuration, is well documented in most electronic texts. Conduction is permitted through the diodes; and then the negative portion of the input can be effectively flipped by the bridge configuration. In addition, similar to the previous ingenious way, a node M is introduced, and one contact-separation cycle is divided into two half cycles [31]. So that, each half cycle becomes a unidirectional charging step, which is beneficial to analyze the charging behavior.

Based on Eqs. (S22)–(S32), systematically numerical calculations of this nonlinear time-variant charging system were carried out aimed at studying the basic charging performances including the current, and power outputs under different C_L. The initial condition we utilized is still the same with the analysis of unidirectional charging. The detailed profiles of the charge, current, and power relationships in the first two cycles are depicted in Fig. 4a-c. In the first half cycle, when the top electrode moves from $x = 0$ to $x = x_{max}$ (Fig. S3a), the voltage across the C_L increases. Conversely, it changes in opposite direction, and can increase continuously because of the full-bridge rectifier. The corresponding variations of the current and charge are shown in Fig. 4b, S5a and S5b, respectively. Moreover, the power is always positive in the duration of the current pulse, which means that energy is continuously being stored in the C_L. When the current returns to zero, the stored energy is trapped because the ideal capacitor offers no means for dissipating energy. Thus a voltage

remains on the C_L even the capacitor current becomes zero. A similar analysis can be conducted for the 2th cycle. Fig. 4d shows the voltage $|V_K^C|$ across the C_L in the first 2th charging cycles, the continued increasing of the voltage is due to the full-bridge rectifier.

As stated before, under a unidirectional motion, the energy stored in C_L could be represented by *V-Q* plots. Herein, this method is utilized under a periodic mechanical motion. As depicted in Fig. 4e, the *V-Q* plot for C_L is a straight line, even after 2 operation cycles, meaning the change tendency of charges stored in C_L is similar to that of the voltage across it. From Eqs. (S23) and (S25), we find the equation $V_K^C/Q_K^C = 1/C_L$, which suggests that the slope of the straight line equals to the reciprocal of C_L. This result can be proved further in Fig. 4f, from which we note that the smaller the loaded C_L, the larger slope of the *V-Q* plot, proving evidence for the above theoretical prediction. In addition, the related charging voltage, charge, current, and power are depicted in Fig. S6, and S7 respectively. Therefore, this new tool presented here can not only provide the detailed charging behavior of TENGs, but also reveal the energy stored in C_L in an easily visible way.

In general, the instantaneous power to C_L can be obtained by finding the product of the voltage and current at any instant of time (Eq. (5) and (S31)). The energy stored in C_L is represented through integrating the output power at a given time (Eqs. (S6) and (S32)). To verify those theoretical predictions continuously, numerical calculations are carried out at different cycle numbers, as shown in Fig. 5.

The power and stored energy for different C_L after 100 charging cycles are shown in Fig. 5a and d. When C_L is small (3 nF), its peak power increases quickly, and then decreases monotonically to its steady-state value, generating a maximum peak power. When C_L is large (10 μF), its peak power keeps growing at a low rate. Then, a $C_{L,opt}$ for maximum peak power can be observed for fixed charging cycles, which is similar to the previous unidirectional charging step. Nevertheless, the energy in C_L is continuously being stored, in the form of an electric field between the conducting surfaces (Fig. 5d). For a given x_{max}, if the k becomes larger, the optimum power increases with a
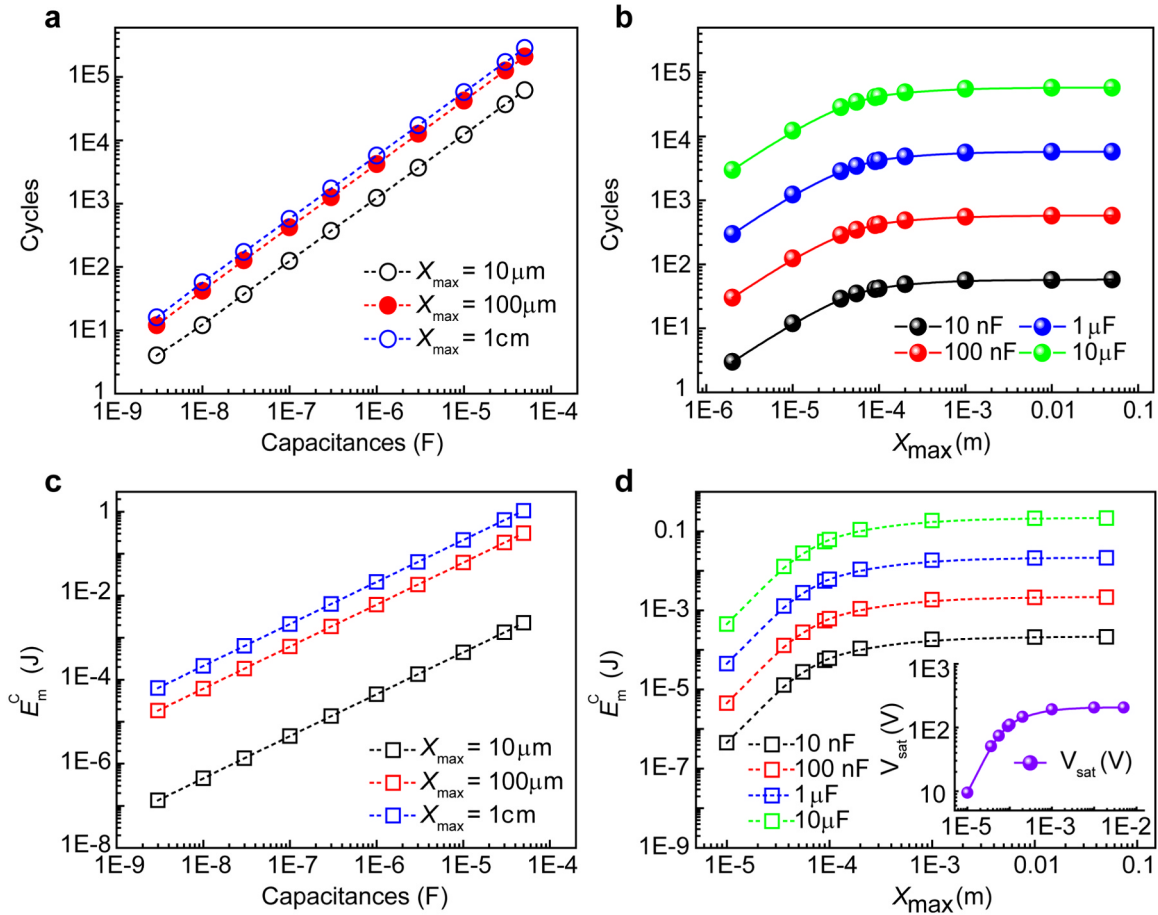
Fig. 6. Upon reaching the saturation voltage V_{sat}, (a) relationship between the final cycle k and load capacitance C_L at different x_{max}, and (b) relationship between the final cycle k and x_{max} at different C_L; (c) relationship between the maximum stored energy E_m^C and C_L at different x_{max}, and (d) relationship between the maximum stored energy E_m^C and x_{max} at different C_L. The inset in (d) shows the relationship between the V_{sat} and x_{max} at different C_L.

decreasing rate until a threshold value is reached, as shown in Fig. 5b (when k approaches 1500, the basic charging performances are demonstrated in Fig. S8). The inset in Fig. 5b shows the relationship between the peak power and C_L at different cycles. This is mainly because the voltage across C_L starts to saturate when k gets large, especially when it goes to infinity. Mathematically, according to Eq. (5) and (S31), when the voltage across C_L approaches V_{sat}, the charging rate reduces, meaning the derivative of the voltage with respect to time t becomes slower, *i.e.*, the factor dV_K^C/dt gets smaller, resulting in a saturation optimum power. The influence of k on the maximum stored energy is demonstrated in Fig. 5e. The maximum stored energy increases as k increases, and a log linear tendency between them can be obtained. In other words, this relationship can be represented by a log linear trend. Consequently, we suggest that the saturation trends can be used as indicator in deciding an appropriate k for a given TENG charging system.

In addition, for a given k, (here, $k = 1500$) a peak power exists as the x_{max} changes (Fig. 5c). This attributes to two reasons. First, as the x_{max} increases, C_{min} of the CS mode TNEG changes very little compared to C_{max}, so that the corresponding optimum capacitance $C_{L,opt}$ approximately remains constant (Fig. S9c), simply because $C_{L,opt}$ is mainly determinded by the sum of C_{min} and C_{max} [31]. Thus, the voltage across $C_{L,opt}$ increases and reaches a saturation point, while the current to the $C_{L,opt}$ shows opposite changes under the same condition (Fig. S9a, S9b, and S9d). Consequently, increasing the x_{max} leads to a variation of output power, and a maximum peak power is observed at an appropriate distance (3.6E-5 m in this study). For the same reasons, the energy stored in $C_{L,opt}$ grows with increasing x_{max} and saturates after a certain x_{max} value (Fig. 5f). Hence, except for the TENG structural

parameters, a better understanding of the charging cycle numbers and motion conditions is equally important in enhancing TENG energy conversion and storage.

Considering the practical application of TENGs, the main concern is to reach the saturation voltage V_{sat} of C_L and the maximum stored energy E_m^C. As demonstrated in Fig. 6a, if the C_L reaches its saturation voltage, it is seen that the final charging cycle depends log linearly on the C_L even at different x_{max}. In particular, the final cycle is proportional to the x_{max} at a fixed C_L (Fig. 6b). From Fig. 6c and d, the same phenomenon can be observed for the relationship between E_m^C and C_L or x_{max} when one of the parameter is fixed and the other changed in a certain range. The inset in Fig. 6d depicts the increasing of V_{sat} for C_L at the increase of x_{max}. It should be noticed that the above descriptions are also applicable to other TENGs with different configurations (Fig. S12-S15). This is mainly because a larger C_L load implies a larger charges can be stored, then a larger number of charging cycles are needed at a fixed x_{max}. On the other hand, the changing of x_{max} at a fixed C_L strongly affects the C_{min} of TENGs, so the V_{sat} and E_m^C and the charging cycle numbers will change also (Eqs. (S6) and (S32)).

4.4. Structural FOMC$_S$ of TENGs

As indicated in Eq. (8), through the maximum stored energy E_m^C in C_L at the final cycle divided by the cycle number taken to achieve the final cycle, the average energy storage in C_L per cycle can be obtained, which has more practical meaning of TENGs for comparison. The calculated structural FOMC$_S$ for the four basic modes of TENGs were compared and depicted in Fig. 7 (detailed parameters are shown in Supplementary tables S3-S5). Edge effects are also considered for the
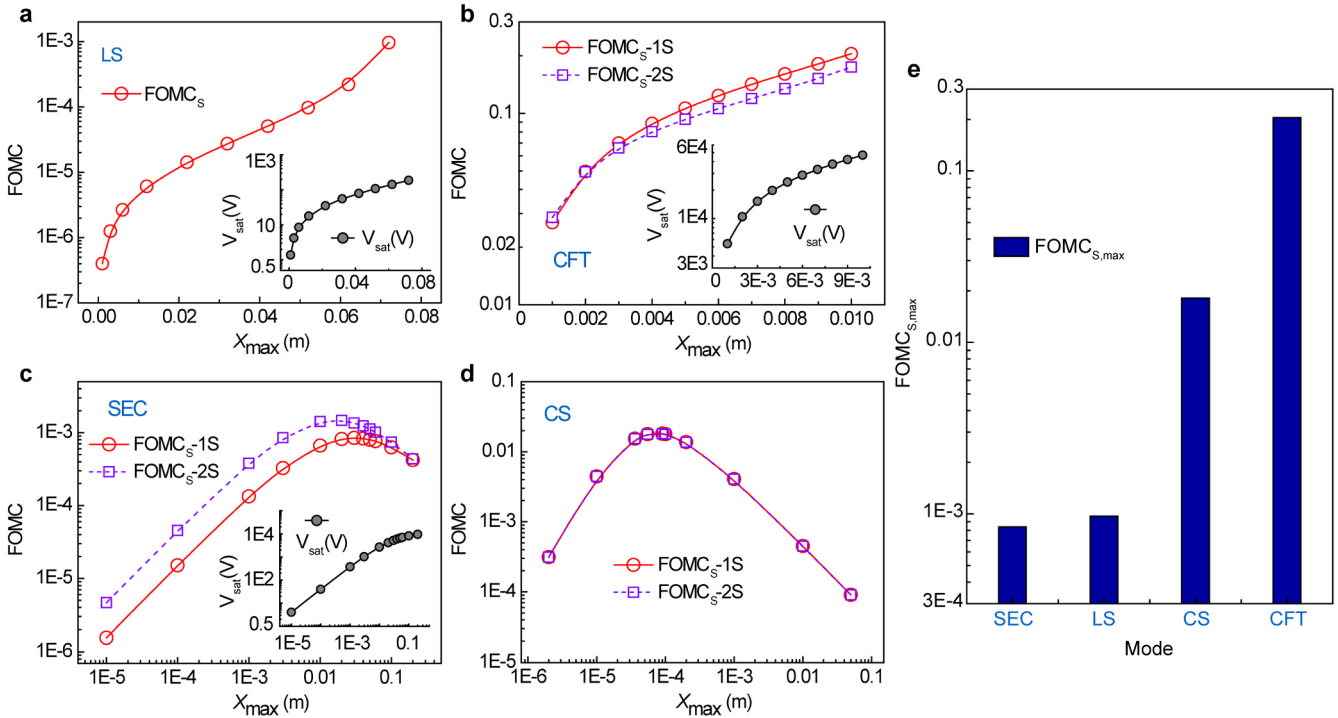
Fig. 7. $FOMC_S$ versus x_{max} for four different TENG modes in a charging system. The FOMC for (a) lateral sliding (LS) structure, (b) contact freestanding triboelectric-layer (CFT) structure, (c) single-electrode contact (SEC) structure and (d) CS mode TENG calculated by analytical formulas. (e) Comparison of extracted maximum structural FOMC ($FOMC_S$, max) for the four basic modes of TENGs. The insets show the saturation voltage of the different load capacitance in the final charging cycles. 1 S and 2 S correspond to calculations considering 1-side and 2-side side effects of the TENGs.

Table 1
Parameters utilized in the numerical calculations for the CS mode TENG.

Structure component	Parameter utilized
Dielectric effective thickness, $d_0 = \Sigma d_i / \varepsilon_i$	3.676E-5 m
Width of Dielectrics, w	7.6223356 cm
Length of Dielectrics, l	7.6223356 cm
Surface charge density, σ	50 μC m^{-2}
Maximum separation distance, x_{max}	2E-6-0.01 m
Velocity, v	1E-4-10 m/s

CFT, SEC and CS mode TENG (Fig. 7b-d) and the corresponding equations are shown in Supplementary Note 5.

Several general conclusions can be extracted from these predictions. First, the structural $FOMC_S$ almost have a similar shape and trend compared with the FOM_S (a correlative formula is given in Supplementary Note 6, detail FOM_S shown in Ref. [41]) under the same conditions, but the former are lower than the latter as can be seen clearly from the extracted maximum values shown in Fig. 7e. That's because the available E_m^C stored in C_L is usually smaller than the ideal E_m in a TENGs system per cycle. Second, the charging performance of TENGs driven by the vertical motion (for instance, the CFT and CS mode) is better than that of the lateral sliding motion (LS mode). The main reason for this is that the LS mode TENG has a bigger inherent capacitance at the same range of x_{max} when compared to other types of TENGs [32,41]. Consequently, for a given transferred charges Q, the larger inherent capacitance leads to a lower E_m^C, making a smaller $FOMC_S$ under the same x_{max}. Physically, the most effective way to do mechanical work by separating oppositely charged surfaces is to separate them in the direction perpendicular to the surface [37]. Finally, the highest $FOMC_S$ for CFT mode TENG is mainly contributed to its double-side triboelectric dielectric film, which is helpful to output larger charges [27]. Instead, the minimum $FOMC_S$ occurring in the SEC mode stems from its single electrode, which limits the total charge transfer and results in a lower voltage.

More importantly, we should note that the structural $FOMC_S$ of TENGs are independent of the C_L. For instance, increasing C_L will increase the maximum stored energy E_m^C, thus resulting in an almost unchanged FOMC shown in the Fig. S11, S12(d), S13(d), and S14(d). To further validate the theoretical predictions presented above, experiments were carried out as demonstrated in Fig. S15. It is seen that our theoretical predictions closely follow the experimental outcomes, providing evidence regarding the accuracy of the TENG power equation and the accompanying assumptions. In particular, because the theoretical investigations are mainly based on the work done by Niu et al., who have demonstrated that their model accurately predicts the charging behaviors of TENGs. Hence, further experiment studies are not carried out here.

5. Conclusions

A comprehensive study of the structural figure of merits of TENGs utilized in energy storage systems (the capacitor as the energy storage unit) is presented based on Maxwell's displacement current, aimed at establishing a future standard for the charging characteristics of TENGs. According to the distance-dependent electric field model, the generation of Maxwell's displacement current and its affecting parameters are discussed qualitatively and extensively. The I_D in the dielectric or between two oppositely charged surfaces is precisely equal to the conduction current in the external circuit for continuity.

From this perspective, the stage-by-stage charging process including unidirectional and periodic mechanical motions are demonstrated, revealing that the transfer of power and energy from a TENG to an external capacitor significantly relays on the load capacitance, charging cycle numbers, and maximum distance x_{max}. It is shown that an optimum capacitance exists which matches the inherent capacitance of TENGs for the maximum peak power and energy stored. Increasing the charging cycle numbers, the optimum power rapidly increases until a saturation value and a log linear trend between the maximum stored

energy and cycle numbers is observed. Finally, through the energy stored in the final charging cycle (at saturation voltage), the structural figure of merits in a TENG charging system (FOMC$_S$) are derived systematically. The analysis can thus be regarded as a standard tool to assess a TENG's charging performances. This work not only establishes an in-depth understanding of the nature of the Maxwell displacement current in a TENG, it also provides an unambiguous evaluation that can be used to operate TENGs more efficiently in an energy storage system. (Table 1)

Acknowledgements

Appendix A. Supplementary material

Supplementary data associated with this article can be found in the online version at doi:10.1016/j.nanoen.2019.02.051.

References

[1] J.C.. Maxwell, Philosophical magazine and journal of science, London, Edinburg and Dubline, Fourth series, p.161.
[2] R. Collin, Field Theory of Guided Waves, Mcgraw-hill, NY, 1960, pp. 1–5.
[3] F.R. Fan, Z.Q. Tian, Z.L. Wang, Flexible triboelectric generator, Nano Energy 1 (2012) 328–334.
[4] H. Ryu, J.H. Lee, U. Khan, S.S. Kwak, R. Hinchet, S.W. Kim, Sustainable direct current powering a triboelectric nanogenerator via a novel asymmetrical design, Energy Environ. Sci. 11 (2018) 2057–2063.
[5] L.C. Luo, D.C. Bao, W.Q. Yu, Z.H. Zhang, T.L. Ren, A low input current and wide conversion ratio buck regulator with 75% efficiency for high-voltage triboelectric nanogenerators, Sci. Rep. 6 (2016) 19246.
[6] Z.L. Wang, Triboelectric nanogenerators as new energy technology and self-powered sensors - principles, problems and perspectives, Faraday Discuss. 176 (2014) 447–458.
[7] H. Ryu, J.H. Lee, T.Y. Kim, U. Khan, J.H. Lee, S.S. Kwak, H.J. Yoon, S.W. Kim, High performance triboelectric nanogenerators based on solid polymer electrolytes with asymmetric pairing of ions, Adv. Energy Mater. 7 (2017) 1700289.
[8] Z.L. Wang, On Maxwell's displacement current for energy and sensors: the origin of nanogenerators, Mater. Today 20 (2017) 74–82.
[9] J. Lowell, A.C. Rose-Innes, Contact electrification, Adv. Phys. 29 (1980) (947-203).
[10] C. Liu, A.J. Bard, Electrostatic electrochemistry at insulators, Nat. Mater. 7 (2008) 505–508.
[11] L.S. McCarty, G.M. Whitesides, Electrostatic charging due to separation of ions at interfaces: contact electrification of ionic electrets, Angew. Chem. Int. Ed. 47 (2008) 2188–2207.
[12] H.T. Baytekin, A.Z. Patashinski, M. Branicki, B. Baytekin, S. Soh, B.A. Grzybowski, The mosaic of surface charge in contact electrification, Science 333 (2011) 308–312.
[13] C. Xu, Y. Zi, A.C. Wang, H. Zou, Y. Dai, X. He, P. Wang, Y.C. Wang, P. Feng, D. Li, Z.L. Wang, On the electron-transfer mechanism in the contact-electrification effect, Adv. Mater. 30 (2018) 1706790.
[14] J. Liu, A. Goswami, K. Jiang, F. Khan, S. Kim, R. McGee, Z. Li, Z. Hu, J. Lee, T. Thundat, Direct-current triboelectricity generation by a sliding Schottky nano-contact on MoS2 multilayers, Nat. Nanotechnol. 13 (2018) 112–116.
[15] Z.L. Wang, T. Jiang, L. Xu, Toward the blue energy dream by triboelectric nanogenerator networks, Nano Energy 39 (2017) 9–23.
[16] J.H. Kim, J. Chun, J.W. Kim, W.J. Choi, J.M. Baik, Self-powered, room temperature electronic nose based on triboelectrification and heterogeneous catalytic reaction, Adv. Funct. Mater. 25 (2015) 7049–7055.
[17] Y. Zhu, B. Yang, J. Liu, X. Wang, L. Wang, X. Chen, C. Yang, A flexible and bio-compatible triboelectric nanogenerator with tunable internal resistance for powering wearable devices, Sci. Rep. 6 (2016) 22233.
[18] Z. Su, J. Chen, Z. Wu, Y. Jiang, Low temperature dependence of triboelectric effect for energy harvesting and self-powered active sensing, Appl. Phys. Lett. 106 (2015) 013114.
[19] M.L. Seol, J.H. Woo, S.B. Jeon, D. Kim, S.J. Park, J. Hur, Y.K. Choi, Vertically stacked thin triboelectric nanogenerator for wind energy harvesting, Nano Energy 14 (2015) 201–208.
[20] B. Meng, W. Tang, Z.H. Too, X. Zhang, M. Han, W. Liu, H.X. Zhang, A transparent single-friction-surface triboelectric generator and self-powered touch sensor, Energy Environ. Sci. 6 (2013) 3235–3240.
[21] W. Xu, L.B. Huang, M.C. Wong, L. Chen, G. Bai, J. Hao, Environmentally friendly hydrogel-based triboelectric nanogenerators for versatile energy harvesting and self-powered sensors, Adv. Energy Mater. 7 (2016) 1601529.
[22] B. Yang, W. Zeng, Z.H. Peng, S.R. Liu, K. Chen, X.M. Tao, A fully verified theoretical analysis of contact-mode triboelectric nanogenerators as a wearable power source, Adv. Energy Mater. 6 (2016) 600505.
[23] Y. Zi, H. Guo, J. Wang, Z. Wen, S. Li, C. Hu, Z.L. Wang, An inductor-free auto-power-management design built-in triboelectric nanogenerators, Nano Energy 31 (2017) 302.
[24] X. Yang, W.A. Daoud, Design parameters impact on output characteristics of flexible hybrid energy harvesting generator: experimental and theoretical simulation based on a parallel hybrid model, Nano Energy 50 (2018) 794–806.
[25] S.M. Niu, Y. Liu, S.H. Wang, L. Lin, Y.S. Zhou, Y.F. Hu, Z.L. Wang, Theoretical investigation and structural optimization of single-electrode triboelectric nano-generators, Adv. Funct. Mater. 24 (2014) 3332–3340.
[26] S.M. Niu, S.H. Wang, L. Lin, Y. Liu, Y.S. Zhou, Y.F. Hu, Z.L. Wang, Theoretical study of contact-mode triboelectric nanogenerators as an effective power source, Energy Environ. Sci. 6 (2013) 3576–3583.
[27] S. Niu, Z.L. Wang, Theoretical systems of triboelectric nanogenerators, Nano Energy 14 (2015) 161–192.
[28] R.D.I.G. Dharmasena, K.D.G.I. Jayawardena, C.A. Mills, R.A. Dorey, S.R.P. Silva, A unified theoretical model for triboelectric nanogenerators, Nano Energy 48 (2018) 391–400.
[29] R.D.I.G. Dharmasena, K.D.G.I. Jayawardena, C.A. Mills, J.H.B. Deane, J.V. Anguita, R.A. Dorey, S.R.P. Silva, Triboelectric nanogenerators: providing a fundamental framework, Energy Environ. Sci. 10 (2017) 1801–1811.
[30] Y. Zi, J. Wang, S. Wang, S. Li, Z. Wen, H. Guo, Z.L. Wang, Effective energy storage from a triboelectric nanogenerator, Nat. Commun. 7 (2016) 10987.
[31] S. Niu, Y. Liu, Y.S. Zhou, S. Wang, L. Lin, Z.L. Wang, Optimization of triboelectric nanogenerator charging systems for efficient energy harvesting and storage, IEEE Trans. Ind. Electron. 62 (2015) 641–647.
[32] J. Shao, W. Tang, X. Chen, L. Xu, Z.L. Wang, Structural figure-of-merits of triboelectric nanogenerators at powering loads, Nano Energy 51 (2018) 688–697.
[33] C. Yao, X. Yin, Y. Yu, Z. Cai, X. Wang, Chemically functionalized natural cellulose materials for effective triboelectric nanogenerator development, Adv. Funct. Mater. 27 (2017) 1700794.
[34] X.S. Zhang, M.D. Han, R.X. Wang, F.Y. Zhu, Z.H. Li, W. Wang, H.X. Zhang, Frequency-multiplication high-output triboelectric nanogenerator for sustainably powering biomedical microsystems, Nano Lett. 13 (2013) 1168–1172.
[35] J.W. Lee, H.J. Cho, J. Chun, K.N. Kim, S. Kim, C.W. Ahn, I.W. Kim, J.Y. Kim, S.W. Kim, C. Yang, J.M. Baik, Robust nanogenerators based on graft copolymers via control of dielectrics for remarkable output power enhancement, Sci. Adv. 3 (2017) e1602902.
[36] Q. Liang, Q. Zhang, X. Yan, X. Liao, L. Han, F. Yi, M. Ma, Y. Zhang, Recyclable and green triboelectric nanogenerator, Adv. Mater. 29 (2017) 1604961.
[37] J. Peng, S.D. Kang, G.J. Snyder, Optimization principles and the figure of merit for triboelectric generators, Sci. Adv. 3 (2017) eaap8576.
[38] B.A. Grzybowski, A. Winkleman, J.A. Wiles, Y. Brumer, G.M. Whitesides, Electrostatic self-assembly of macroscopic crystals using contact electrification, Nat. Mater. 2 (2003) 241–245.
[39] R. Elsdon, F.R.G. Mitchell, Contact electrification of polymers, J. Phys. D Appl. Phys. 9 (1976) 1445.
[40] B.A. Kwetkus, Particle triboelectrification and its use in the electrostatic separation process, Part Sci. Technol. 16 (1998) 55–68.
[41] Y. Zi, S. Niu, J. Wang, Z. Wen, W. Tang, Z.L. Wang, Standards and figure-of-merits for quantifying the performance of triboelectric nanogenerators, Nat. Commun. 6 (2015) 8376.